ACADEMIC PRESS

Available online at www.sciencedirect.com

SCIENCE DIRECT®

Journal of Sound and Vibration 268 (2003) 385–401

JOURNAL OF SOUND AND VIBRATION

www.elsevier.com/locate/jsvi

Time-domain numerical computation of noise reduction by diffraction and finite impedance of barriers

Chang Woo Lim, Cheolung Cheong, Seong-Ryong Shin, Soogab Lee*

Institute of Advanced Aerospace Technology, School of Mechanical and Aerospace Engineering, Seoul National University, Seoul 151-742, South Korea

Received 25 June 2001; accepted 21 November 2002

Abstract

A new time-domain numerical method is presented for the estimation of noise reduction by the diffraction and finite impedance of barriers. High order finite difference schemes conventionally used for computational aeroacoustics, and time-domain impedance boundary conditions are utilized for the development of the time-domain method. Compared with other methods, this method can be applied more easily to the problems related to nonlinear noise propagation such as impulsive noise and broadband noise. Linearized Euler equations in Cartesian co-ordinates are considered and solved numerically. Straight and T-shaped barriers with and without surface admittance are calculated. In order to assess the accuracy of this time-domain method, comparison with the results of SYSNOISE software (Ver. 5.3) are made. There are very good agreements between the results of the present time-domain numerical method and the boundary element method of the SYSNOISE software.

1. Introduction

The increasing magnitude and types of noise generated by road traffic in modern city life have aroused much interest in the problem of noise pollution, initiating the development of numerical techniques and simulations concerned with noise reduction measures. One of the simplest and most effective measures in open space is a suitably shaped and placed absorbing acoustic barrier. Many methods have been presented to predict the performance of the noise barriers. They can be classified into three categories, namely, scale-model or full-scale experiments, theoretical approaches, and wave-based numerical methods.

*Corresponding author. School of Mechanical and Aerospace Engineering, Seoul National University, San 56-1, Shilim-Dong, Kwanak-Gu, Seoul 151-742, South Korea. Tel.: +82-2-880-7384; fax: +82-2-887-2662.

E-mail address: solee@plaza.snu.ac.kr (S. Lee).

0022-460X/03/$ - see front matter
doi:10.1016/S0022-460X(02)01534-1

Experimental approaches are often used to solve the practical problems including atmospheric conditions and complex interactions. Scholes et al. [1] performed an experiment with full-scale barriers on grass-covered ground. May and Osman [2] examined a number of new barrier models promising improved performance using a 1/16 scale model experiment. Experimental approaches, however, are more expensive than analytic and numerical methods.

Numerous theoretical techniques have been developed for the prediction of the performance of the noise barriers. Many of them are based on geometrical ray theory and the diffraction theory of acoustic waves extended from the optical diffraction theory. These techniques are based on energy methods and thus ignore phase difference. One of the simplest and most widely used methods is Maekawa's empirical diffraction model [3] that provides the insertion loss due to a thin-wall barrier in terms of the Fresnel number. Kawai et al. [4] developed a simple, approximate expression for Bowman and Senior's formula, which is based on Macdonald's rigorous solution, again by using the Fresnel number. Pierce [5], Jonasson [6] and Tolstoy [7] improved more sophisticated mathematical methods for determining the barrier diffraction caused by a two-dimensional angle or a polygonal line. Kurze and Anderson [8] and Kurze [9] discussed the use of Keller's geometrical theory for the asymptotic form of the counterpart of Sommerfeld's solution for determining the diffraction of complex barrier shapes in the shadow zone. L'Esperance [10] proposed a simple method for estimating the insertion loss of a finite-length barrier. Jonasson [11], Chessell [12] and Isei [13] proposed methods for calculating the noise reduction of a barrier on the ground of finite impedance. Lam and Roberts [14] introduced a method for the calculation of the acoustic energy loss produced by the insertion of simple, finite-length, three-dimensional acoustic barriers. These theoretical approaches, however, cannot deal with the barriers of complex geometry causing multi-diffraction effects.

Common numerical approaches to estimate barrier performance are wave-based numerical methods such as the finite element method (FEM) and the boundary element method (BEM). The wave-based methods solve wave equations, i.e., the Helmholtz equation and thus exactly model reflection, diffraction and phase interference in the sound field around barriers. Filippi and Dumery [15] and Terai [16] developed a boundary integral equation technique to analyze the scattering of sound waves by thin rigid screens in the unbounded regions. Seznec [17] and Hothersall et al. [18] solved two-dimensional diffraction problems for rigid barriers above a rigid plane and absorbing barriers above an impedance plane, respectively. Duhamel and Sergent [19] calculated a sound pressure around the acoustic barrier of an arbitrary cross-section placed over the absorbing rigid ground, and compared the obtained numerical results with the experimental data. Morgan et al. [20] assessed the influence of the shape and absorbent surface of railway noise barriers, using a two-dimensional boundary element model. More recently, Jean et al. [21] computed the efficiency of noise barriers, considering the different source types such as point sources, coherent and incoherent line sources. BEM, however, has some difficulties in solving the problems that include the propagation of broadband or nonlinear noise.

The objective of this paper is to develop a time-domain numerical method as an alternative numerical tool for the prediction of the barrier's efficiency. One of the significant advantages of time-domain methods over frequency-domain methods is that the problems containing broad-band-noise or nonlinear noise propagation can be handled relatively easily.

In contrast to the computational fluid dynamics (CFD) that has advanced to a fairly mature state, computational aeroacoustics (CAA) has only recently come forth as a separate area of

study. Aeroacoustics problems are governed by the same equations as aerodynamics, but acoustic waves have their own characteristics that make their computation more challenging. Acoustic waves are intrinsically unsteady, and their amplitudes are several order smaller than the mean flow of the very high frequency. Distances from the noise source to the boundary of the computation domain are also usually quite long. Thus, to ensure that computed solutions are uniformly accurate over such long propagation distances, numerical schemes must be free of numerical dispersion, dissipation and anisotropy. To satisfy these requirements, a high order numerical scheme in both space and time is generally required for CAA. Recent reviews of CAA by Tam [22] and Wells and Renaut [23] have discussed various numerical schemes currently popular in CAA. These include many compact and non-compact optimized schemes such as the family of high order compact differencing schemes of Lele [24] and dispersion relation preserving (DRP) scheme of Tam and Webb [25]. Recently, impedance boundary conditions in time domain were suggested by Tam and Auriault [26]. These boundary conditions are the equivalent of the frequency-domain impedance boundary conditions. High order finite difference schemes optimized in wave number space, and time-domain impedance boundary conditions are utilized for the development of a new time-domain method.

The outline of this paper is as follows. The new time-domain numerical method, which consists of the high order finite difference scheme and the impedance boundary condition, will be discussed in Section 2. Numerical results for several barriers with locally reacting surface will be presented in Section 3. In order to assess the accuracy of the time-domain numerical results, computational results will be compared with the numerical results of BEM obtained from SYSNOISE software (Ver. 5.3).

2. Time-domain numerical methods

2.1. Optimized finite difference schemes

Two-dimensional linearized Euler equations, governing the propagation of small acoustic disturbances, may be written in a dimensionless form where the reference quantities are Δx for the length scale, c (ambient sound speed) for the velocity scale, therefore $\Delta x/c$ for the time scale, ρ_∞ for the density scale, and $\rho_\infty c^2$ for the pressure scale. The dimensionless linearized Euler equations are as follows:

$$\frac{\partial \mathbf{U}}{\partial t}+\frac{\partial \mathbf{E}}{\partial x}+\frac{\partial \mathbf{F}}{\partial y}=\mathbf{Q}, \tag{1}$$

where

$$\mathbf{U}=\begin{bmatrix}\rho\\ u\\ v\\ p\end{bmatrix},\quad \mathbf{E}=\begin{bmatrix}u\\ p\\ 0\\ u\end{bmatrix},\quad \mathbf{F}=\begin{bmatrix}v\\ 0\\ p\\ v\end{bmatrix},\quad \mathbf{Q}=\begin{bmatrix}S_1\\ S_2\\ S_3\\ S_4\end{bmatrix}.$$

The vector $\mathbf{Q}$ of Eq. (1) represents acoustic sources. The linearized Euler equations in Cartesian co-ordinates are solved by the DRP finite difference scheme. In the wave propagation theory, it is

well known that the propagation characteristics of waves, governed by the linear system of partial differential equations, is determined completely by the dispersion relations. The DRP scheme is designed so that the dispersion relation of the finite difference scheme is the same as that of the original partial differential equations. A seven-point stencil DRP scheme is utilized for spatial discretization. The resolution of the spatial discretization is often represented by the minimum points-per-wavelength needed to resolve a wave reasonably. The minimum points-per-wavelength of a seven-point DRP scheme is 5.4 when using the criterion $|k\Delta x - \bar{k}\Delta x| \leqslant 0.005$ where k and $\bar{k}$ represent the wave numbers of the partial differential equations and finite difference equations, respectively. Optimized 4-level time discretization (Adams–Bashford method) is used as the explicit time marching scheme [23]. The DRP scheme, just as all the other high order finite difference schemes, induces short-wavelength spurious numerical waves. These spurious waves are often generated at the computation boundaries and interfaces by non-linearity. They are the pollutants of the numerical solutions. When the excessive amount of spurious waves is produced, it does not lead only to the quality degradation of the numerical solutions, but also to numerical instability in many instances. To obtain high-quality time-domain numerical solutions, damping is, therefore, essential to eliminate the spurious numerical waves of short wavelength. A conventional method to do this is to add artificial selective damping terms to finite difference equations. Damping terms were designed to eliminate only the short waves proven by Tam et al. [27]. The discretized forms of Eq. (1) using the 7-point stencil DRP scheme, the explicit optimized 4-level time-marching scheme, and the artificial selective damping terms can be expressed in the following forms:

$$K_{l,m}^{(n)} = -\frac{1}{\Delta x}\sum_j a_j E_{l+j,m}^{(n)} - \frac{1}{\Delta y}\sum_j a_j F_{l,m+j}^{(n)} - \frac{L}{\Delta x}\frac{1}{R\,e_{\Delta x}}\sum_j d_j U_{l+j,m}^{(n)} - \frac{L}{\Delta y}\frac{1}{R\,e_{\Delta y}}\sum_j d_j U_{l,m+j}^{(n)} + Q_{l,m}^{(n)}, \tag{2}$$

and

$$U_{l,m,k}^{n+1} = U_{l,m,k}^{n} + \Delta t \sum_{j=0}^{3} b_j K_{l,m,k}^{(n-j)}. \tag{3}$$

The last two terms in Eq. (2) are the artificial damping terms, where d_j is the coefficient of damping stencils and $R\,e_\Delta$ is the mesh Reynolds number ($R\,e_{\Delta x} = c\Delta x/v_a$) that only has the computational meaning.

2.2. Boundary conditions

2.2.1. Farfield boundary condition

For high-quality computed solutions, farfield boundary conditions must sufficiently transmit outgoing disturbances so that they exit from the computational domain without reflection. Waves in the linearized Euler equations are classified into three categories: acoustic, entropy and vorticity waves having distinct wave propagation characteristics, respectively. The acoustic wave consists of all the physical variables and has its own velocity, $u + c$ (mean flow velocity + speed of sound). The entropy wave consists of the density fluctuation alone while the vorticity wave consists of the

velocity fluctuation alone. Since the latter two waves do not have their own velocity, they only move downstream frozen at the mean flow velocity. Without the mean flow velocity, only the acoustic wave goes through the boundary of the computational domain. Therefore, radiation boundary conditions for the acoustic wave are derived from asymptotic solutions of the linearized Euler equations. These radiation boundary conditions are applied and their equations are as follows:

$$\left(\frac{1}{V(\theta)}\frac{\partial}{\partial t}+\frac{\partial}{\partial r}+\frac{1}{2r}\right)\begin{bmatrix}\rho\\ u\\ v\\ p\end{bmatrix}=0, \tag{4}$$

where $V(\theta)=c_0[M\cos\theta+(1-M^2\sin^2\theta)^{1/2}]$, $r=\sqrt{x^2+y^2}$.

2.2.2. Wall boundary condition with finite impedance

2.2.2.1. Modelling of impedance. Impedance is defined as the ratio of the acoustic pressure, p to the acoustic velocity component, v_n normal to the treated surface:

$$Z=p/v_n, \tag{5}$$

where v_n is positive when pointing into the surface. The impedance is determined by a complex quantity, $Z=R'+\mathrm{i}X'$. The use of a complex quantity is needed to account for the damping and phase shift imparted on sound waves by the acoustically treated surface. Theoretical investigations [28,29] have improved the understanding of the influence of the finite impedance surface. For example, soil is not rigid and impervious, but consists of grains of various shapes and sizes. The gaps between grains form pores that are filled with air and/or water. The sound waves impinging on the porous ground surface are partly reflected. Some of the sound energy penetrates into the ground along the air-filled pores, vibrates grains and dissipates due to the viscous friction and thermal exchanges. This mechanism is indicated in Fig. 1. In this work, the model of Delany and Bazley [28] is used to calculate the impedance of surface. The normal surface impedance normalized with respect to characteristic impedance of air ($\rho_0 c$) can be expressed in terms of the dimensionless parameter, $\rho_0 f/\sigma$. Here, ρ_0 (kg/m^3) is the density of air, f (Hz) the frequency, and σ (N s/m^4) the specific flow resistivity per unit thickness of the material. Delany and Bazley also showed that these relations are useful for the calculation of the impedance boundary effect. The Delany and Bazley's empirical relation for the fibrous sound absorbing material can be expressed as follows:

$$\frac{Z_2}{\rho_0 c}=1+0.0571\left(\frac{\rho_0 f}{\sigma}\right)^{-0.754}+\mathrm{i}0.0870\left(\frac{\rho_0 f}{\sigma}\right)^{-0.732}. \tag{6}$$

Fig. 2 shows the comparison between the empirical model Eq. (6) of $\sigma=506$ kN s/m^4 and the measurement data [29] for a lawn. There are good agreements in the normalized resistance and reactance, respectively.

2.2.2.2. Impedance wall boundary conditions. Assuming that the sound field consists of a single frequency ω ($\omega>0$), the pressure and velocity fields of sound waves can be expressed as $p(x,t)=Re[\hat{p}(x)\mathrm{e}^{\mathrm{i}\omega t}]$ and $v(x,t)=Re[\hat{v}(x)\mathrm{e}^{\mathrm{i}\omega t}]$. The normalized impedance is defined as $Z/\rho_0 c=R+\mathrm{i}X$.

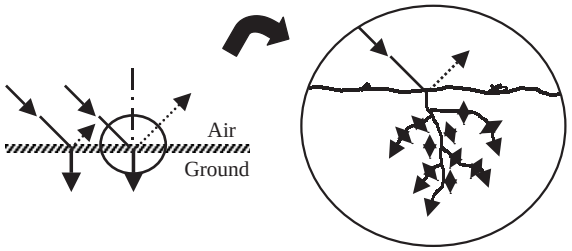

Fig. 1. Air to ground coupling mechanism.

It is designed primarily for frequency-domain analysis. Tam and Auriault [26], however, proposed suitable time-domain impedance boundary conditions that are equivalent to those of the frequency-domain at the wall surface.

For the positive normalized reactance X, the time-domain impedance boundary condition for a single frequency at the surface is

$$p = -Rv - \frac{X}{\omega}\frac{\partial v}{\partial t}, \tag{7}$$

where v is the outward-pointing, normal velocity of the surface ($v = -v_n$). Application of Eq. (1) into Eq. (7) leads to the following relation, which is equivalent to the impedance boundary condition Eq. (7):

$$\frac{\partial p}{\partial y} = \frac{\omega}{X}(p + Rv). \tag{8}$$

This equation provides ghost values at time level $(n+1)$, p_{-1}^{n+1} of the following form:

$$p_{-1}^{n+1} = \frac{\omega \Delta y}{X a_{-1}^{15}}\left((Rv_0^{n+1} + p_0^{n+1}) - \frac{X}{\omega \Delta y}\sum_{j=0}^{5} a_j^{15} p_j^{n+1}\right). \tag{9}$$

For a high order finite difference scheme, the order of the difference equation is higher than that of the Euler equations. Thus, additional numerical conditions must be imposed. The pressure values at the ghost points are used for the extraneous boundary condition at the wall.

To illustrate the accuracy of the time-domain impedance boundary condition, the results of numerical simulation are compared with theoretical solutions in the frequency domain. A single-frequency acoustic-wave train is introduced over the absorbing surface. Sources are sinusoidal coherent line sources, S_1 and S_4 in the Eq. (1). They are given in the following form:

$$S_1 = S_4 = \varepsilon \exp\left[-\ln 2\left(\frac{(x - x_0)^2 + (y - y_0)^2}{r^2}\right)\right]\cos(\omega t). \tag{10}$$

Sound waves are reflected off the acoustically absorbing surface, which is characterized by the flow resistivity, $\sigma = 200$ kN s/m^4. It is equivalent to the property of the grass-covered surface.

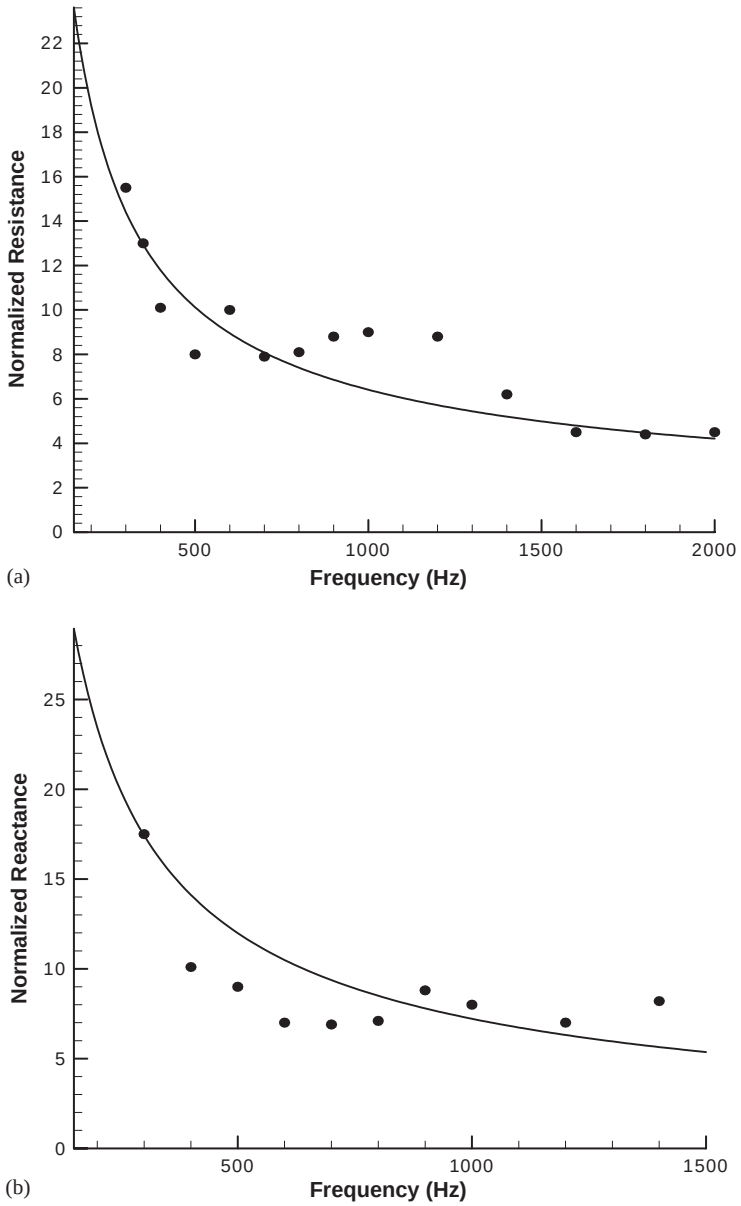

Fig. 2. Comparison between measurements (•) of the normalized surface impedance of lawn (Attenborough) and prediction of Delany and Bazley's empirical equation (—) with $\sigma = 506\,000$MKS units: (a) normalized resistance, (b) normalized reactance.

The values of u and p are updated to the next time level by the Eq. (3) at every point on the grid except ghost point values. Ghost values p_{-1}^{n+1} are calculated by the Eq. (9). Pressure contours over the full computation domain are shown in Fig. 3. In this computation, the source parameters: ε, x_0, y_0, r and ω are set to 1, 0, 0.5, 0.1 and 2000π, respectively. Pressure distributions at the line of

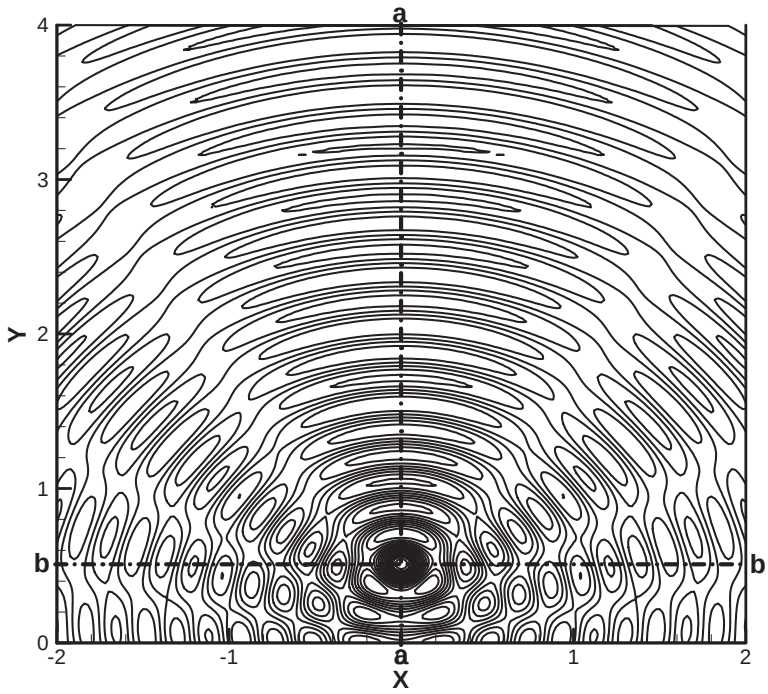

Fig. 3. Pressure contour reflected off absorbing surface defined by $\sigma = 200$ kN s/m^4.

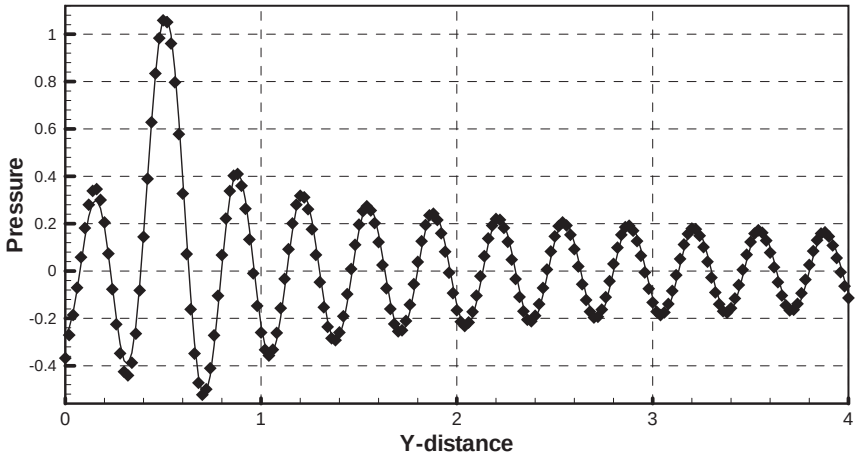

Fig. 4. Spatial pressure distribution along line *a–a* in Fig. 3. —, Time-domain solution; ♦—♦ theoretical solution in frequency domain.

a–a and *b–b* in Fig. 3 are shown in Figs. 4 and 5, respectively. There are good agreements between the numerical and theoretical results. These results suggest that the time-domain solution involving the impedance boundary is feasible and accurate.

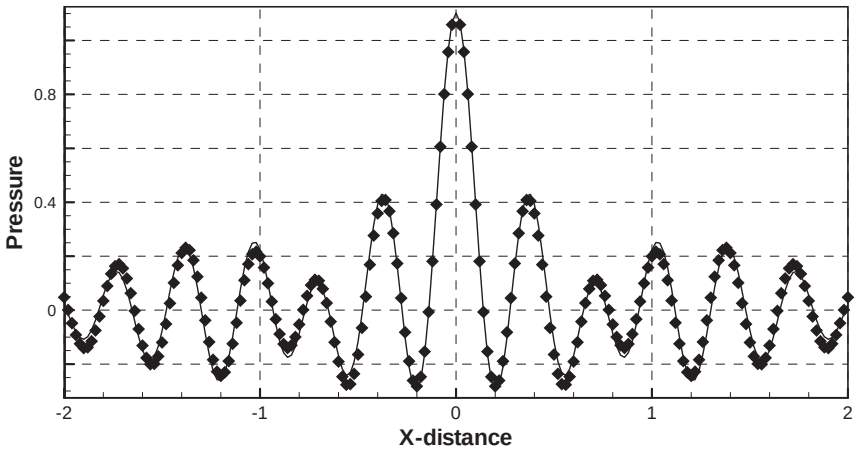

Fig. 5. Spatial pressure distribution along line *b–b* in Fig. 3. —, Time-domain solution; ♦—♦, theoretical solution in frequency domain.

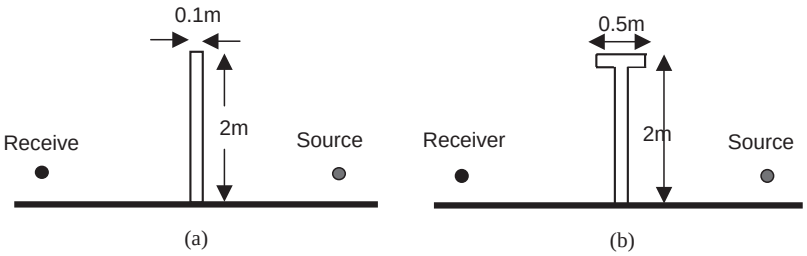

Fig. 6. Barrier geometry: (a) straight barrier, (b) T-shaped barrier. —, Surface of zero-admittance.

3. Numerical simulation for barriers

In order to predict the efficiency of several types of noise barriers, two-dimensional numerical simulations are carried out. Noise sources are assumed to be coherent line sources defined by Eq. (10). The surface of barriers is assumed to have a locally reacting surface. To describe the surface impedance, the empirical model of Delany and Bazley [28] for fibrous materials is used with the flow resistivity, $\sigma = 200$ kN s/m^4. In order to validate numerical solutions in the time-domain method, predicted results are compared with those of SYSNOISE software.

Figs. 6 and 7 show geometries and impedance characteristics of barriers considered in this work. The sound source is 0.5 m above the ground and 1.9 m to the right of the wall at point (2, 0.5). The receiver point is 2 m behind the wall and 0.5 m above the ground at point (−2, 0.5). The origin is always at the bottom left of the wall. The values ε and r of Eq. (10) are set to be 1 and 0.1, respectively. In the following simulations, above-mentioned parameters are kept constant except when noted otherwise.

Figs. 8 and 9 show applied boundary conditions and root mean square (RMS) pressure contours over the full computational domain around the straight barrier and T-shaped barrier, respectively. These plots use a gray scale, ranging from black to white as the amplitude increases.

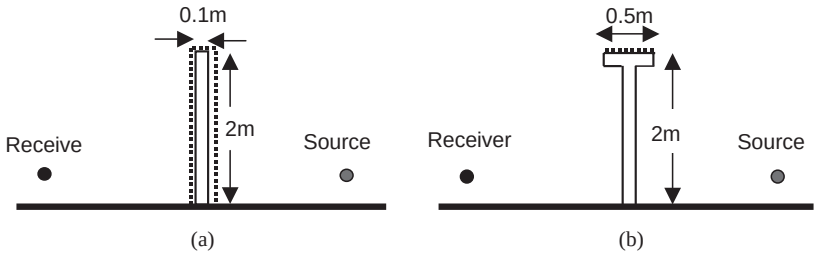

Fig. 7. Barrier geometry: (a) straight barrier, (b) T-shaped barrier. —, surface of zero-admittance; ·····, surface of admittance of $\sigma = 200$ kN s/m^4.

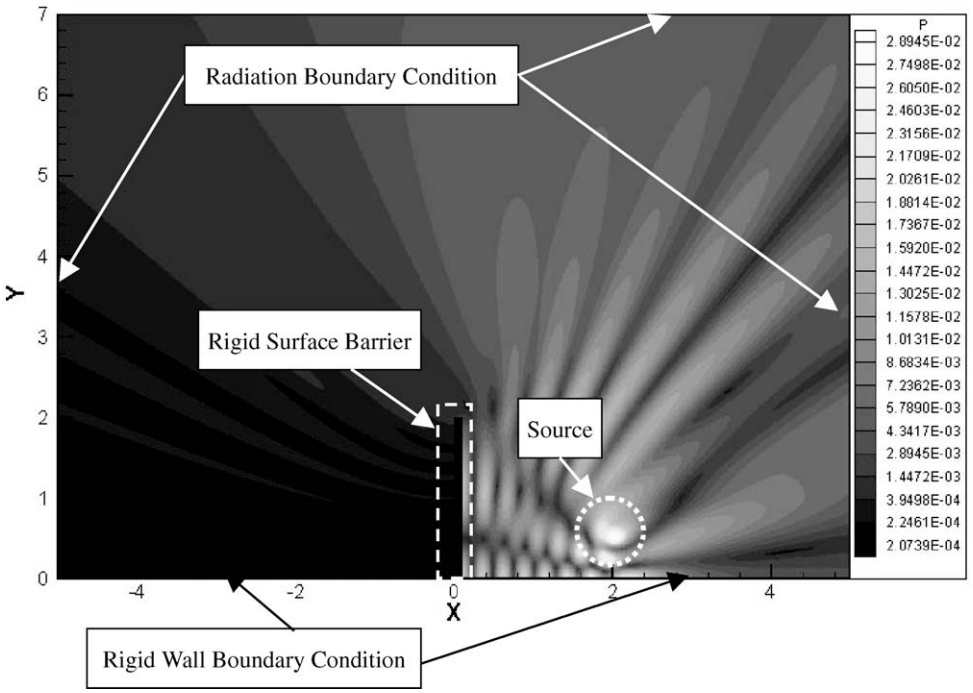

Fig. 8. Boundary conditions and RMS pressure contours around the straight barrier of rigid surface. (The colors change from black to white as the amplitude increases.)

These calculations are carried out with a single-frequency source defined in Eq. (10) with the angular frequency, ω, of 680. If there is no sound-absorbing mechanism on the surface, the only sound-attenuating mechanism is the diffraction at the edge of the barrier. Through the interference between waves diffracted at the edge of the barrier and reflected off the ground, specific wave patterns come into being in the shadow region behind the barrier.

To illustrate the propagation of the general broadband sound, time responses are presented for a 5 m tall barrier. At the time when $t = 0.0$, a Gaussian-like pulse is emitted from a location at $x = 2.5$ m, $y = 2.5$ m, and time responses are calculated when the center frequency of the pulse is 68 Hz.

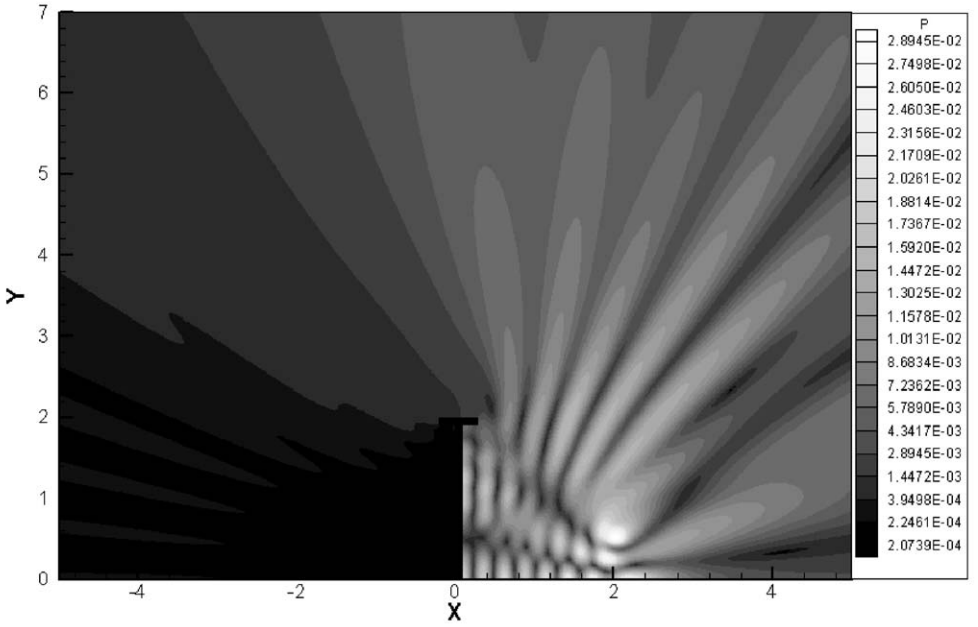

Fig. 9. RMS pressure contours around the T-shaped barrier of rigid surface. (The colors change from black to white as the amplitude increases.)

Fig. 10 shows the sequence of snapshots of pressure wave fields. In this figure, the pressure amplitude is colored with the gray scale, ranging from white to black as the amplitude increases.

As the pulse propagates away from the source, the wave energy spreads out. At the time when $t = 7.4$ ms, the incident pulse reaches the acoustic barrier. As the time progresses, the incident pulse strikes the edge of the barrier at $t = 10.4$ ms and diffracts in all directions, even along the vertical face of the barrier. The time-domain methods have some advantages over the boundary element methods in handling broadband noise problems. [26,30]

Excess attenuation (EA) is generally used to evaluate the efficiency of the acoustic barrier. The excess attenuation is defined as the sound pressure level with a wall divided by the sound pressure level in the free field:

$$EA = 20 \log_{10}(|p_{wall}|/|p_{free}|). \tag{11}$$

In the calculation of the excess attenuation at multiple frequencies through the time-domain numerical method, the noise source in Eq. (10) can be expressed in the following form:

$$S_1 = S_4 = \varepsilon \exp\left[-\ln 2\left(\frac{(x - x_0)^2 + (y - y_0)^2}{r^2}\right)\right] \sum_{i=1}^{35} \cos(\omega_i t). \tag{12}$$

Here, $\omega_i = 85 \times (i - 1) + 170$ (Hz). Then, by applying the Fourier transform to the time-history of the pressure at the receiving point, the excess attenuation at the above frequencies are determined. This approach is available because the linearized Euler equations are used as the governing equations.

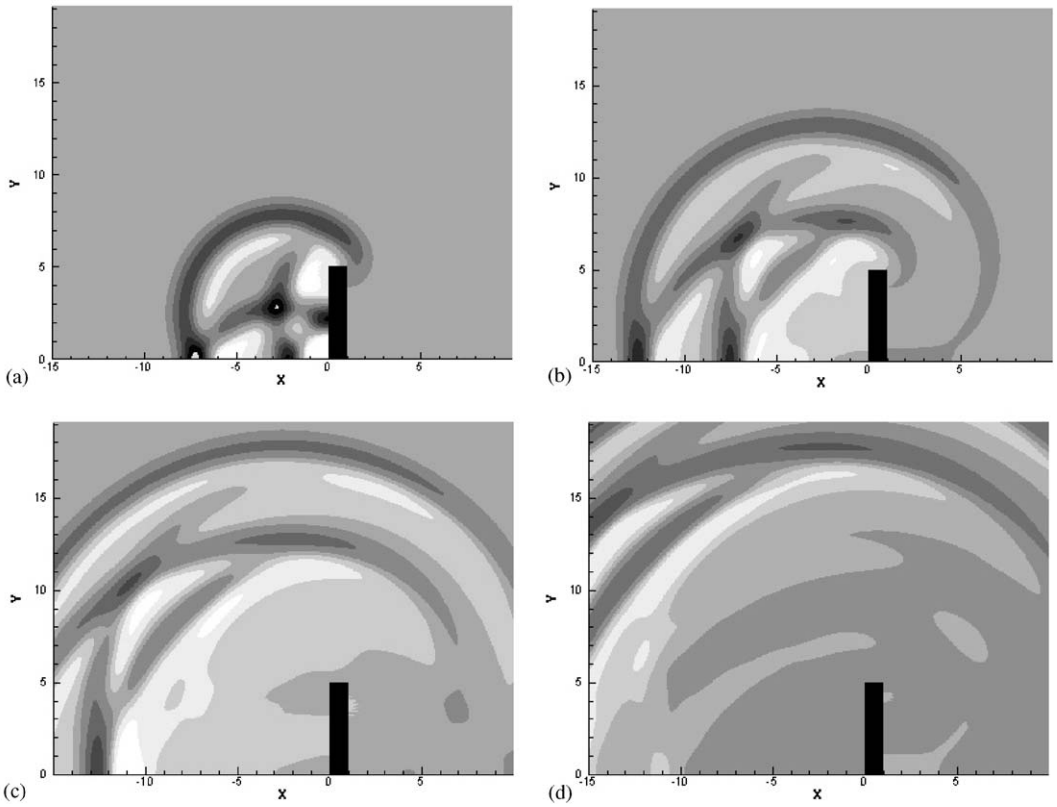

Fig. 10. Time histories over a straight barrier of height, $h = 5.0$ m. (The colors change from black to white as the amplitude increases.) (a) $t = 14.7$ ms, (b) $t = 29.4$ ms, (c) $t = 44.1$ ms, (d) $t = 58.8$ ms.

Figs. 11 and 12 show the computed excess attenuation from the time-domain method and BEM of SYSNOISE software for the straight barrier and T-shaped barrier in Fig. 6, respectively. These computations were carried out with a personal computer (CPU AMD athlon 1.2 GHz, RAM 512 Mb). It takes the time-domain method 6.0×10^4 s to obtain the RMS of sound pressure over the full computation domain for straight barrier with one-frequency source. The BEM of SYSNOISE software requires 1.55×10^3 s to obtain the same result. In order to calculate the excess attenuation of barriers shown in Figs. 11 and 12, multiple frequencies are calculated. Whereas the BEM of SYSNOISE depends on the number of the frequency, the time-domain method is independent because noise sources can be represented by the Eq. (12). The graph in the Fig. 13 represents the time required with respect to the number of frequencies. This figure shows that the necessary time of the time-domain method gets equal to the BEM of SYSNOISE in the same condition when the number of frequencies is about 39.

The excess attenuation of the T-shaped barrier behaves in a more complicated manner with respect to frequency than the straight barrier, because the interferences between waves diffracted by the T-shaped barrier and reflected from the ground become more complex. It is well known that the overall excess attenuation of the T-shaped barrier is greater than that of the straight

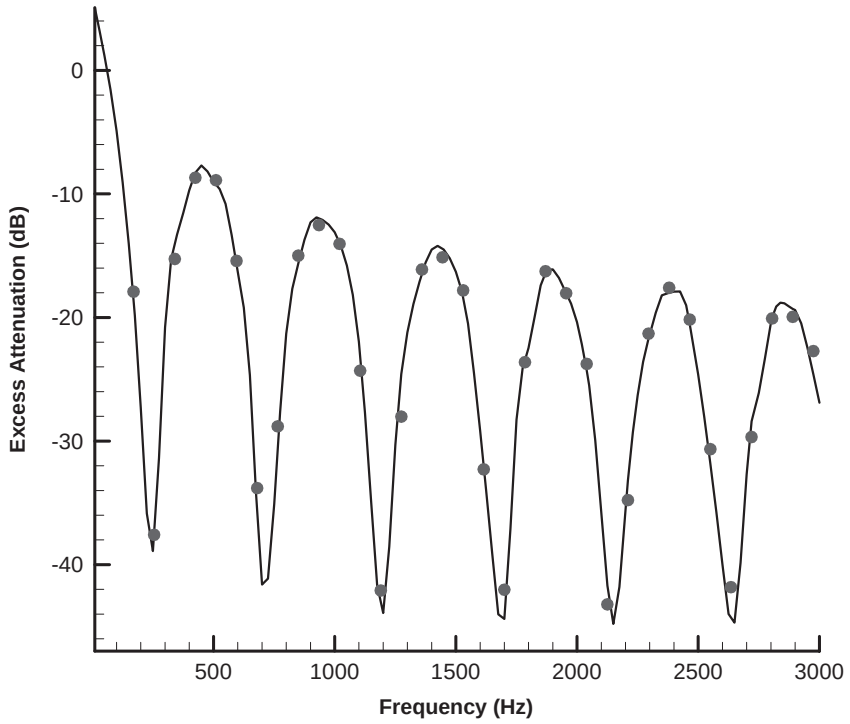

Fig. 11. Excess attenuation of a straight barrier with zero-admittance (case (a) in Fig. 6): —, BEM using SYSNOISE; • , time-domain method.

barrier. This can be explained by the increase in the path difference of the ray from source to receiver and the increase in the diffraction at the edges. There are however, very good agreements between the results of the time-domain numerical computation and the BEM of SYSNOISE software.

Fig. 14 shows the excess attenuation of the straight barrier with and without surface admittance. The flow resistivity of the non-zero surface admittance is set to be $\sigma = 200$ kN s/m^4, which is appropriate for the impedance of a grass-covered surface (an absorbing ground). Because the absorbing surface reduces reflection, the overall attenuation of the absorbing surface is larger than that of the rigid surface. Fig. 15 shows the excess attenuation of the T-shaped barrier with and without top surface admittance. The flow resistivity of non-zero surface admittance is set to be $\sigma = 200$ kN s/m^4, which is the same as that of the straight barrier. Similarly to the case of the straight barrier, the overall attenuation of the T-shaped barrier with top surface admittance is greater than that of the rigid surface. At the low frequencies ($\leqslant 250$ Hz), the effect of the finite impedance of the absorbing barriers is small enough to be almost negligible. As the frequency increases from 250 Hz, the effect of the finite impedance becomes more significant. The T-shaped barrier with absorbing top surface provides more visible improvement in excess attenuation than the straight barrier with full absorbing surface. This performance enhancement has also been reported by the model experiments [2] and the BEM approach [31].

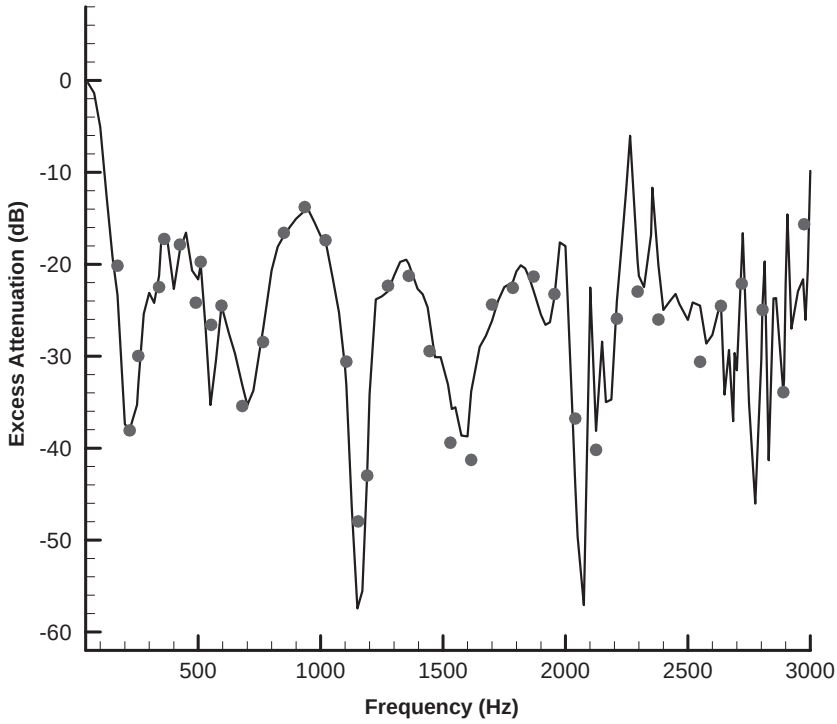

Fig. 12. Excess attenuation of a T-shaped barrier with zero-admittance (case (b) in Fig. 6): —, BEM using SYSNOISE ; •, time-domain method.

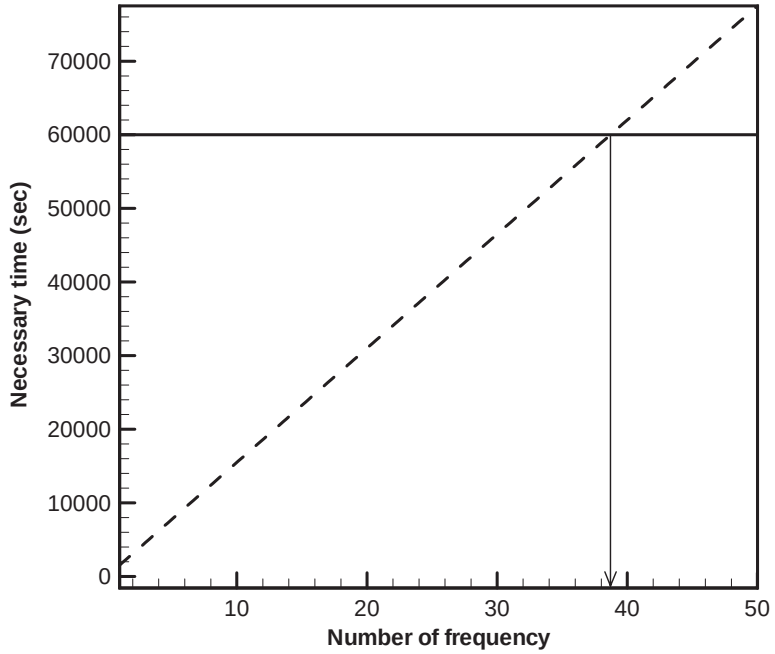

Fig. 13. Necessary time with respect to number of frequencies. —, time-domain method; - - -, BEM of SYSNOISE.

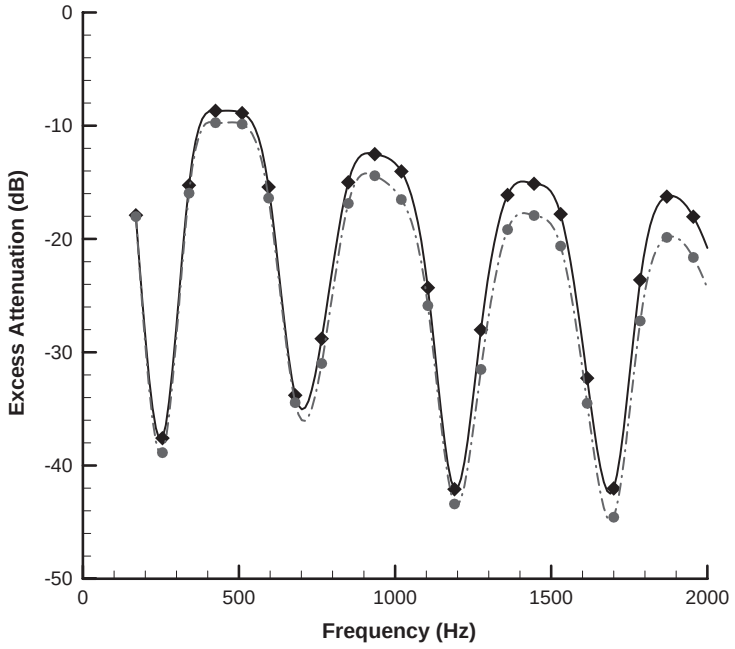

Fig. 14. Excess attenuation for a straight barrier with surface admittance zero ($\sigma = \infty$) and an admittance defined by $\sigma = 200$ kN s/m^4 (case (a) in Figs. 6 and 7): ♦—♦, rigid surface barrier; ●·····●, absorbing surface barrier.

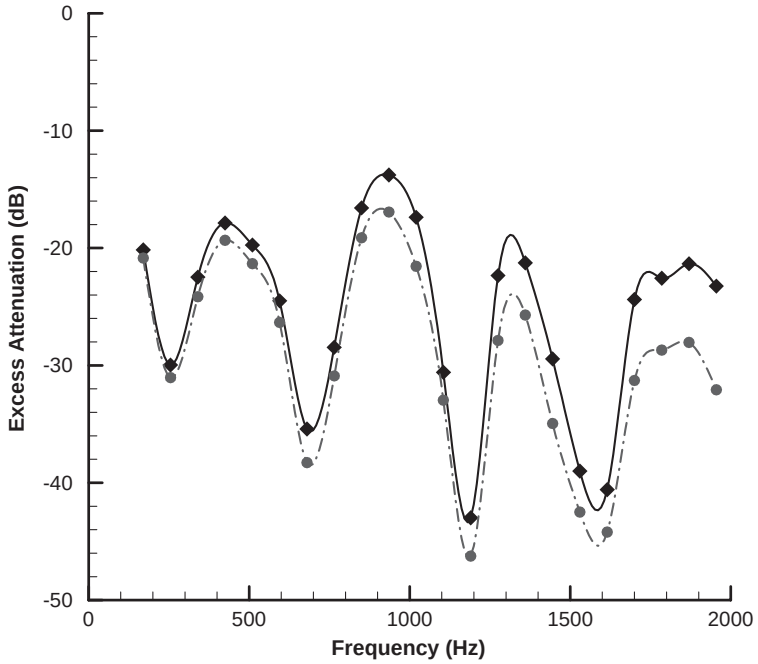

Fig. 15. Excess attenuation for a T-shaped barrier with surface admittance zero ($\sigma = \infty$) and an admittance defined by $\sigma = 200$ kN s/m^4 (case (b) in Figs. 6 and 7): ♦—♦, rigid surface barrier; ●·····●, absorbing surface barrier.

4. Concluding remarks

A new time-domain numerical method was proposed as a powerful numerical tool to calculate the sound propagation around the acoustic barriers with absorbing surfaces. Through the comparison of the computational results with those of the BEM, the accuracy of the time-domain method was verified.

Although the main purpose of this work is to develop the time-domain method and to validate its accuracy, it is evident that the time-domain method has some advantages over boundary element methods. This time-domain method can handle broadband noise problems more easily. This approach can also be applied to the problems containing nonlinear noise propagation phenomena, and especially to impulsive-noise problems. Considering the merits of the time-domain numerical method, it is clear that the method offers an alternative way to solve the problems that the boundary element methods previously found it difficult to approach.

Future work will be aimed at applying the time-domain method to the noise barrier problems containing high-intensity impulsive-noise sources, in which nonlinear noise propagation are important and broadband noise at the receiving point is concerned.

Acknowledgements

This work was sponsored by the Research Institute of Engineering Science and Brain Korea 21 Project.

References

[1] W.E. Scholes, A.C. Salvidge, J.W. Sargent, Field performance of a noise barrier, Journal of Sound and Vibration 16 (1971) 627–642.
[2] D.N. May, M.M. Osman, Highway noise barriers: new shapes, Journal of Sound and Vibration 71 (1980) 73–101.
[3] Z. Maekawa, Noise reduction by screens, Applied Acoustics 1 (1968) 157–173.
[4] T. Kawai, K. Fujimoto, T. Itow, Noise propagation around a thin half plane, Acustica 38 (1978) 313–323.
[5] A.D. Pierce, Diffraction of sound around corners and over wide barriers, Journal of the Acoustical Society of America 55 (1974) 941–955.
[6] H.G. Jonasson, Diffraction by wedges of finite acoustic impedance with applications to depressed roads, Journal of Sound and Vibration 25 (1972) 577–585.
[7] I. Tolstoy, Exact, explicit solutions for diffraction by hard sound barriers and seamounts, Journal of the Acoustical Society of America 85 (1989) 661–669.
[8] U.J. Kurze, G.S. Anderson, Sound attenuation by barriers, Applied Acoustics 4 (1971) 35–53.
[9] U.J. Kurze, Noise reduction by barriers, Journal of the Acoustical Society of America 55 (1974) 504–518.
[10] A. L'Esperance, The insertion loss of finite length barriers on the ground, Journal of the Acoustical Society of America 86 (1989) 179–183.
[11] H.G. Jonasson, Sound reduction by barriers on the ground, Journal of Sound and Vibration 22 (1972) 113–126.
[12] C.I. Chessell, Propagation of noise along a finite impedance boundary, Journal of the Acoustical Society of America 62 (1977) 825–834.
[13] T. Isei, Absorptive noise barrier on finite impedance ground, Journal of the Acoustical Society of Japan 1 (1980) 3–10.

[14] Y.M. Lam, S.C. Roberts, A simple method for accurate prediction of finite barrier insertion loss, Journal of the Acoustical Society of America 93 (1993) 1445–1460.
[15] P. Filippi, G. Dumery, Étude théorique et numérique de la diffraction par un écran mince, Acustica 21 (1969) 343–359.
[16] T. Terai, On calculation of sound fields around three-dimensional objects by integral equation methods, Journal of Sound and Vibration 69 (1980) 71–100.
[17] R. Seznec, Diffraction of sound around barriers: use of the boundary elements technique, Journal of Sound and Vibration 73 (1980) 195–209.
[18] D.C. Hothersall, S.N. Chandler-Wilde, M.N. Hajmirzae, Efficiency of single noise barriers, Journal of Sound and Vibration 146 (1991) 303–322.
[19] D. Duhamel, P. Sergent, Sound propagation over noise barriers with absorbing ground, Journal of Sound and Vibration 218 (1998) 799–823.
[20] P.A. Morgan, D.C. Hothersall, S.N. Chandler-Wilde, Influence of shape and absorbing surface—a numerical study of railway barriers, Journal of Sound and Vibration 217 (1998) 405–417.
[21] P. Jean, J. Defrance, Y. Gabillet, The importance of source type on the assessment of noise barriers, Journal of Sound and Vibration 226 (1999) 201–216.
[22] C.K. Tam, Computational aeroacoustics: issues and methods, American Institute of Aeronautics and Astronautics Journal 33 (1995) 1788–1796.
[23] V.L. Wells, R.A. Renaut, Computing aerodynamically generated noise, Fluid Mechanics 29 (1997) 161–199.
[24] S.K. Lele, Compact finite difference schemes with spectral-like resolution, Journal of Computational Physics 103 (1992) 16–42.
[25] C.K.W. Tam, J.C. Webb, Dispersion-relation-preserving finite difference schemes for computational acoustics, Journal of Computational Physics 107 (1997) 262–281.
[26] C.K.W. Tam, L. Auriault, Time-domain impedance boundary conditions for computational aeroacoustics, American Institute of Aeronautics and Astronautics Journal 34 (1996) 917–923.
[27] C.K.W. Tam, J.C. Webb, Z. Dong, A study of the short wave components in computational acoustics, Journal of Computational Acoustics 1 (1993) 1–30.
[28] M.E. Delany, E.N. Bazley, Acoustical properties of fibrous absorbent materials, Applied Acoustics 3 (1976) 105–116.
[29] K. Attenborough, Acoustical impedance models for outdoor ground surfaces, Journal of Sound and Vibration 99 (1985) 521–544.
[30] Y. Ozyoruk, L.N. Long, M.G. Jones, Time-domain numerical simulation of a flow-impedance tube, Journal of Computational Physics 146 (1998) 29–57.
[31] K. Fujiwara, D.C. Hothersall, C.H. Kim, Noise barriers with reactive surfaces, Applied Acoustics 53 (1997) 255–272.